Electrochemistry Communications 156 (2023) 107575

Contents lists available at ScienceDirect

Electrochemistry Communications

journal homepage: www.elsevier.com/locate/elecom

Short Communication

Reductive deposition of aluminum at a water-free ionic liquid/oil interface

Naohiro Yoshida, Yohei Kuroyama, Yuko Yokoyama, Tetsuo Sakka, Naoya Nishi *

Department of Energy and Hydrocarbon Chemistry, Kyoto University, Kyoto 615-8510, Japan

ARTICLE INFO

Keywords:
ITIES
Ionic liquid/oil interface
Electroless deposition

ABSTRACT

The oil/water interface has been used as a reaction field for interfacial metal deposition via electron transfer between metal ions and reducing agents across the interface. However, the metals that can be deposited at liquid/liquid interfaces are limited to noble metals whose standard redox potential is more positive than that of water. In the present study, we designed a water-free liquid/liquid interface between a hydrophilic ionic liquid (IL) and oil (O) and succeeded in reductively depositing Al, a base metal that has a significantly negative standard redox potential and that is not reduced at water-based liquid/liquid interfaces. The morphology of the deposited Al was investigated and the reaction mechanism was explained as a combination of electron transfer and ion transfer across the IL/O interface.

1. Introduction

Immiscible liquid/liquid interfaces such as oil (O)/water (W) interfaces have been studied as useful reaction fields for the fabrication of metal nanostructures [1–19]. In a liquid–liquid two-phase system, a reducing agent dissolved in only one phase can be separated from a metal precursor dissolved in only the other phase, so the reaction field for the redox reaction between them can be limited to the liquid/liquid interface [2]. This spatial restriction allows us to fabricate metal nanostructures with various morphologies, including not only nanoparticles but also nanorods [7], nanoplates [8], nanowires [5], and nanoshells [13]. Recently, ionic liquids (ILs) have been attracting attention as a new class of solvents that could be used as alternatives to water and oil. ILs are salts that are liquid near room temperature and have properties such as a wide potential window, non-volatility, flame resistance, and ionic conductivity. We have designed an IL/W interface using hydrophobic ILs instead of oil as a reaction field for the reductive deposition of noble metals such as Au [10], Ag [15], Pd [14], and Pt [11], and successfully fabricated nanostructures such as dendritic nanofibers of noble metals at the interface. However, reductive deposition of metals at O/W and IL/W interfaces is limited to noble metals whose standard reduction potentials are more positive than that of water; base metals such as Zn and Al have more negative standard reduction potentials and therefore their reduction is hindered by water reduction.

To overcome this limitation, we have designed a water-free IL/O interface for base metal deposition. We have reported that this IL/O interface can be used as an electrochemical reaction field [17]. We have succeeded in the reductive deposition of the base metal Zn, which cannot be deposited at W/O and W/IL interfaces [18]. In the present study, we further explore base metal deposition in the IL–O two-phase system, focusing on Al, which has a more negative standard reduction potential than Zn. Al nanostructures show promise for applications in photodetection, sensing, and plasmon-enhanced photocatalysis [20–25]. Although reductive deposition of Al in a one-phase system has been reported [26–31], to the best of our knowledge Al reduction at a liquid/liquid interface has not yet been achieved. Here, we report the successful preparation of Al nanostructures at a water-free IL/O interface and propose a reaction mechanism based on ^{27}Al-NMR measurements.

2. Experimental

1-(3-hydroxypropyl)-3-methylimidazolium chloride (C_{3OH}mimCl) was used as the IL phase [17,18]. $AlCl_3$ (Fujifilm Wako Pure Chemical) was dissolved in C_{3OH}mimCl at a mole fraction $x_{AlCl_3}\left(=n_{AlCl_3}/\left(n_{AlCl_3}+n_{IL}\right)\right)=0.67$. A toluene solution of 1 M diisobutylaluminium hydride ($^{i}Bu_2AlH$, TCI Chemicals), a reducing agent, was used as the oil phase. C_{3OH}mimCl was prepared using 3-chloro-1-propanol and 1-methylimidazole, following a procedure described in a previous paper [32]. C_{3OH}mimCl was dried in vacuo for at least three days before use, and all the following processes were carried out under a N_2 atmosphere. The redox reaction was initiated by gently pouring the oil (5 mL) onto the ionic liquid (2.5 g) in a round flask, where $^{i}Bu_2AlH$ is

* Corresponding author.
E-mail address: nishi.naoya.7e@kyoto-u.ac.jp (N. Nishi).

https://doi.org/10.1016/j.elecom.2023.107575
Received 16 August 2023; Received in revised form 31 August 2023; Accepted 4 September 2023
Available online 5 September 2023
1388-2481/© 2023 The Author(s). Published by Elsevier B.V. This is an open access article under the CC BY license (http://creativecommons.org/licenses/by/4.0/).

the limiting reactant for the reaction. The liquid–liquid two-phase system was left under a N_2 atmosphere at 75 °C for 24 h. Deposits formed at the IL/O interface were collected by repeated centrifuging and washing cycles with toluene, acetonitrile, and tetrahydrofuran, all of which were of anhydrous grade.

The deposits were analyzed on a copper foil with SEM/EDX apparatus (an EMAXEvolution X-Max (80 mm^2) HORIBA-equipped SU8200 (Hitachi)). XRD measurements were performed with a SmartLab 3 kW/HP/MLT (Rigaku). After the reaction, the oil phase was taken in a quartz NMR tube for ^{27}Al-NMR measurements. A D_2O solution of 1.5 M Al $(NO_3)_3$ was used as a standard. Toluene solutions of $^{i}Bu_2AlH$, $^{i}BuAlCl_2$, and $^{i}Bu_2AlCl$ were also measured in the same way to identify the reaction products. The toluene solutions of $^{i}BuAlCl_2$ and $^{i}Bu_2AlCl$ were prepared by adding $AlCl_3$ to $^{i}Bu_3Al$ (1 M toluene solution, Fujifilm Wako Pure Chemical) in the molar ratios 1:2 and 2:1, respectively.

3. Results and discussion

Immediately after the two-phase formation, bubbles were generated and gray deposits appeared at the IL/O interface. The gases produced were found to be hydrogen and isobutane, as identified by gas detector tubes. The generation of hydrogen gas can be explained by the oxidation reaction of the reducing agent $^{i}Bu_2AlH$ (see Eq. (3) below) and the generation of isobutane by the hydrolysis reaction of $^{i}Bu_2AlH$ (see Eq. (1)).

$$^{i}Bu_2AlH\ (O) + 2H_2O\ (IL) \rightarrow {}^{i}BuAl(OH)_2\ (O) + H_2\uparrow + CH(CH_3)_3\uparrow \quad (1)$$

Karl Fischer titration confirmed 1000 ppm water in the ionic liquid, which caused the hydrolysis of $^{i}Bu_2AlH$. A calculation indicated that this is a minor reaction; only 0.6% of the reducing agent iBu_2AlH would be consumed even if all the water in the IL were to react. Indeed, no reaction products from the hydrolysis were detected in the analyses described below (^{27}Al-NMR, EDX, XRD).

Fig. 1(a) shows an SEM image of the deposits collected after the 24 h reaction. The deposits have a branch-like structure whose typical size is 1 μm. The deposits were confirmed to be metallic Al by EDX (Fig. 1b) and XRD (Fig. 1c) measurements. The crystallite size, τ, was estimated from the full width at half maximum, β, of each peak in the X-ray pattern using the Scherrer equation (Eq. (2).

$$\tau = \frac{K\lambda}{\beta\cos\theta} \quad (2)$$

where K is the shape factor (0.9), λ is the X-ray wavelength (an intensity-weighted average ($2 \times 1.540562 + 1.544398$)/3 = 1.54184 Å of the $CuK\alpha_1$ and $CuK\alpha_2$ lines), and θ is the Bragg angle. The estimated crystallite size of deposited Al was 40 nm.

In the following, we discuss the Al reduction process. The oxidation reaction of $^{i}Bu_2AlH$ can be written as:

$$2\,{}^{i}Bu_2AlH\ (O) \rightarrow 2\ {}^{i}Bu_2Al^{+}\ (O) + H_2\uparrow + 2e^{-} \quad (3)$$

Possible reduction reactions of Al precursors are given in Eqs. (4) and (5):

$$4Al_2Cl_7^{-}\ (IL) + 3e^{-} \rightarrow Al + 7AlCl_4^{-}\ (IL) \quad (4)$$

$$AlCl_4^{-}\ (IL) + 3e^{-} \rightarrow Al + 4Cl^{-}\ (IL) \quad (5)$$

According to the literature for C_2mimCl/$AlCl_3$ (x_{AlCl_3} = 0.67) at 40 °C, the anionic species in the IL are $AlCl_4^{-}$, $Al_2Cl_7^{-}$, and $Al_3Cl_{10}^{-}$, at fractions of 0.1, 0.8, and 0.1, respectively [33] and similar fractions are expected in C_{3OH}mimCl. In addition, the reduction potentials of $Al_2Cl_7^{-}$, and $AlCl_4^{-}$, in C_2mimCl-$AlCl_3$ (x_{AlCl_3} = 0.67) are 0 and − 1.3 V (vs. Al), respectively [34], indicating that $AlCl_4^{-}$, is unlikely to undergo reduction reactions. We indeed confirmed that deposition does not occur in the case of x_{AlCl_3} = 0.25, where $AlCl_4^{-}$ is the only Al-related species in the IL. Therefore, the $Al_2Cl_7^{-}$ reduction (Eq. (4)) is the reaction occurring in the present reaction system. As a whole, the redox reaction in which oxidation (Eq. (3)) and reduction (Eq. (4)) occur at the same time at the

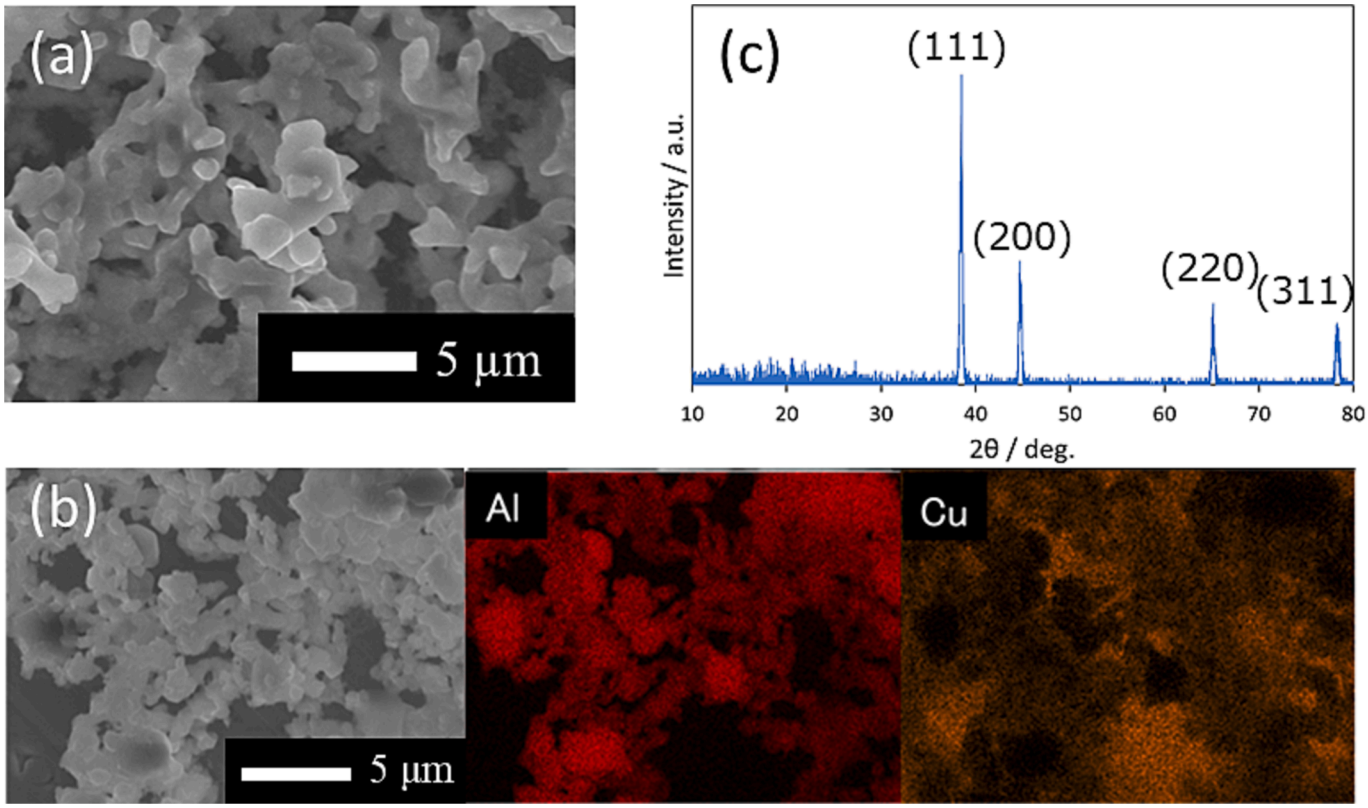

Fig. 1. (a) SEM image, (b) EDX mapping (on a Cu foil), and (c) XRD pattern of the deposited Al.

IL/O interface can be regarded as an electron transfer (ET) across the IL/O interface from O to IL.

$$6\,{}^{i}Bu_2AlH\ (O) + 8Al_2Cl_7^-\ (IL) \rightarrow 2Al + 3H_2\uparrow + 6\,{}^{i}Bu_2Al^+\ (O) + 14AlCl_4^-\ (IL) \quad (6)$$

Simultaneously with ET, ion transfer (IT) should occur to maintain the electroneutrality of each liquid phase in the present electroless condition. Since ${}^{i}Bu_2Al^+$ generated by the oxidation reaction of ${}^{i}Bu_2AlH$ (Eq. (3)) is a strong Lewis acid, it will react with Lewis bases: anions in the present system. Therefore, the following four anion transfers from IL to O, which are facilitated with ${}^{i}Bu_2Al^+$ via Lewis acid–base reactions, can be considered.

$$\text{IT1: } {}^{i}Bu_2Al^+\ (O) + Cl^-\ (IL) \rightarrow {}^{i}Bu_2AlCl\ (O) \quad (7)$$

$$\text{IT2: } {}^{i}Bu_2Al^+\ (O) + AlCl_4^-\ (IL) \rightarrow 2\,{}^{i}BuAlCl_2\ (O) \quad (8)$$

$$\text{IT3: } {}^{i}Bu_2Al^+\ (O) + Al_2Cl_7^-\ (IL) \rightarrow 2\,{}^{i}BuAlCl_2\ (O) + AlCl_3\ (O) \quad (9)$$

$$\text{IT4: } {}^{i}Bu_2Al^+\ (O) + Al_3Cl_{10}^-\ (IL) \rightarrow 2\,{}^{i}BuAlCl_2\ (O) + 2AlCl_3\ (O) \quad (10)$$

IT1, IT2, IT3, and IT4 are ITs from IL to O for Cl^-, $AlCl_4^-$, $Al_2Cl_7^-$, and $Al_3Cl_{10}^-$, respectively. It should be noted that Cl^- does not exist in the IL under the condition where $x_{AlCl_3} = 0.67$, however, the equilibrium between two existing Al species can generate Cl^- to be transferred to O, such as $2AlCl_4^- \rightleftharpoons Al_2Cl_7^- + Cl^-$. There are also possible ITs in which ${}^{i}Bu_2Al^+$ is transferred from O to IL, as exemplified by IT1′ below:

$$\text{IT1}': {}^{i}Bu_2Al^+\ (O) + 2Cl^-\ (IL) \rightarrow {}^{i}Bu_2AlCl_2^-\ (IL) \quad (11)$$

To investigate which of the ITs shown above actually occur, the Al-related species in the O-phase after the reaction were characterized using ^{27}Al-NMR. Fig. 2 shows the ^{27}Al-NMR spectra for the O phase before (blue) and after (red) the reaction. The spectrum before the reaction shows a broad peak centered at 160 ppm that can be assigned to ${}^{i}Bu_2AlH$. After the reaction, the signal was shifted upfield and has two peaks: a broad one at 126 ppm and a sharp one at 95 ppm. To identify the reaction products, toluene solutions of two possible species ${}^{i}BuAlCl_2$ and ${}^{i}Bu_2AlCl$ (see Eqs. (7)–(10)), were also tested. The corresponding spectra (Fig. 2) showed peaks with the same positions and width as those in the spectrum after the reaction (see Table 1). These results suggest that IT1 and IT2 generated ${}^{i}BuAlCl_2$ and ${}^{i}Bu_2AlCl$ in the oil phase during the reaction. Apart from NMR, we also confirmed that $AlCl_3$ cannot be dissolved in toluene at a detectable amount, indicating that IT3 and IT4 are unlikely to occur.

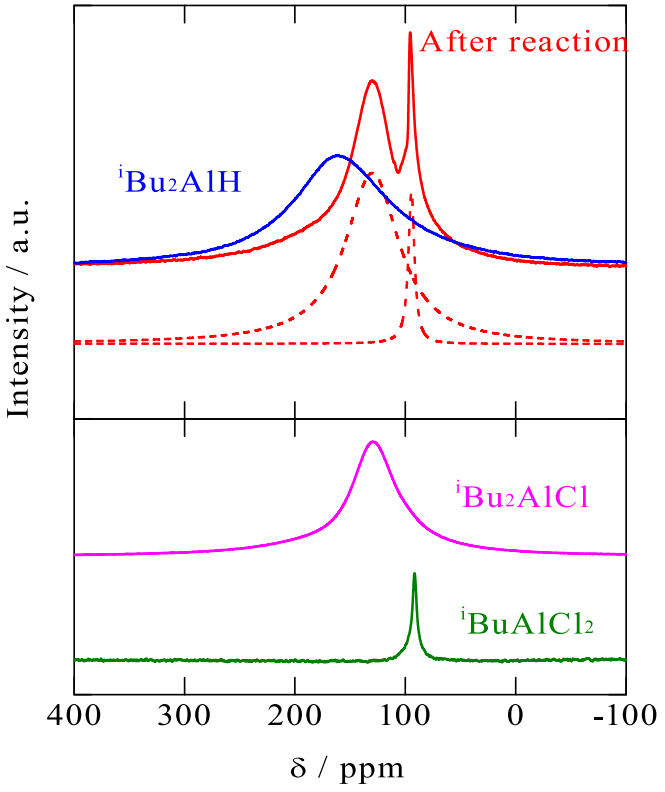

Fig. 2. ^{27}Al-NMR spectra for the O phase before (blue) and after (red) reductive deposition of Al at the IL/O interface, and for toluene solutions of ${}^{i}Bu_2AlCl$ (pink) and ${}^{i}BuAlCl_2$ (green). The red dashed lines show the deconvolution into two peaks by fitting with the Lorentz function from the spectrum after the reaction. (For interpretation of the references to colour in this figure legend, the reader is referred to the web version of this article.)

For a quantitative discussion, the obtained NMR spectra were fitted using the Lorentz function. The spectrum of the oil phase after the reaction was successfully fitted by two peaks (red dashed lines in Fig. 2). The deconvoluted two peaks were attributed to ${}^{i}Bu_2AlCl$ and ${}^{i}BuAlCl_2$ with peak areas of 0.83 and 0.10, relative to that of ${}^{i}Bu_2AlH$ before the reaction. The peak area indicates that the main dissolved species after the reaction is ${}^{i}Bu_2AlCl$. The peaks of ${}^{i}Bu_2AlCl$ and ${}^{i}BuAlCl_2$, the reaction products of IT1 and IT2, were observed, indicating that IT1 and IT2 occurred, with the former playing the major role. The peak area sum of the two peaks after the reaction was 0.93, which is smaller than unity, the peak area before the reaction. This means that the Al content of the oil decreased due to the reaction and suggests that Al-related species were transferred from O to IL, as exemplified by IT1′ (Eq. (11)). However, this transfer is minor compared to the ion transfer IT1 from IL to O.

Based on the above results, we propose a mechanism of Al reductive deposition as shown in Fig. 3. The electron transfer between ${}^{i}Bu_2AlH$ and $Al_2Cl_7^-$ produces metallic Al and hydrogen gas. IT1 mainly occurs to counterbalance the charge bias due to the electron transfer. ${}^{i}Bu_2Al^+$, an intermediate Al-related species generated in the oil phase via electron transfer, facilitates transfer of Cl^- from IL to O, generating ${}^{i}Bu_2AlCl$ in the oil.

4. Conclusions

Reductive deposition of the base metal Al was successfully achieved at a water-free IL/O interface. ^{27}Al-NMR measurements identified Al-related species generated during the reaction and confirmed the reaction mechanism. Electrochemical measurements of this system at the IL/toluene interface would further reveal the charge transfer reactions, as was done at the W/toluene interface by Kasuno and coworkers [36,37]. This fundamental water-free IL–O system could be extended by introducing potential control and capping reagents to aid the formation of base metal nanostructures that show attractive application properties. This approach could also be applied to the deposition of other base

Table 1
Parameters from the ^{27}Al-NMR measurements.

	Present study			Literature [35]	
	δ (ppm)	Peak area [c]	Peak width	δ (ppm)	Peak width
${}^{i}Bu_2AlH$ (1 M) (O phase before the reaction)	160	1	54 ppm 5600 Hz	159 [a]	9000 Hz [a]
O phase after the reaction	126	0.83	26 ppm 2700 Hz	–	–
	95	0.10	3.6 ppm 380 Hz	–	–
${}^{i}Bu_2AlCl$	128	–	27 ppm 2800 Hz	173 [b]	4270 Hz [b]
${}^{i}BuAlCl_2$	91.6	–	3.0 ppm 310 Hz	–	–

[a] $({}^{i}Bu_2AlH)_3$ in Toluene-d_8.
[b] $({}^{i}Bu_2AlCl)_2$ in Toluene-d_8.
[c] Normalized by the ${}^{i}Bu_2AlH$ peak.

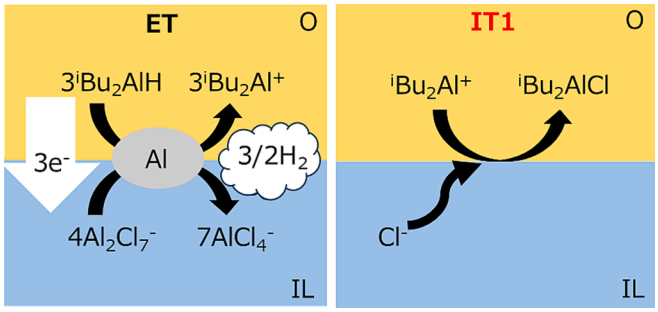

Fig. 3. Reaction mechanism for Al deposition at the IL/O interface.

metals by designing appropriate metal precursors and reducing agents.

CRediT authorship contribution statement

Naohiro Yoshida: Investigation, Writing – original draft. **Yohei Kuroyama:** Investigation. **Yuko Yokoyama:** Writing – review & editing. **Tetsuo Sakka:** Writing – review & editing. **Naoya Nishi:** Conceptualization, Writing – review & editing, Supervision, Project administration, Funding acquisition.

Declaration of Competing Interest

The authors declare that they have no known competing financial interests or personal relationships that could have appeared to influence the work reported in this paper.

Data availability

Data will be made available on request.

Acknowledgments

This work was partly supported by the Japan Society for the Promotion of Science (JSPS) KAKENHI Grants (21H02046, 23H03829). We acknowledge Eriko Kusaka for the ^{27}Al-NMR measurements.

References

[1] M. Guainazzi, G. Silvestri, G. Serravalle, J. Chem. Soc., Chem. Commun. (1975) 200–201.
[2] Y. Cheng, D.J. Schiffrin, J. Chem. Soc. Faraday Trans. 92 (1996) 3865–3871.
[3] R.M. Lahtinen, D.J. Fermín, H. Jensen, K. Kontturi, H.H. Girault, Electrochem. Commun. 2 (2000) 230–234.
[4] R.A.W. Dryfe, A.O. Simm, B. Kralj, J. Am. Chem. Soc. 125 (2003) 13014–13015.
[5] F. Scholz, U. Hasse, Electrochem. Commun. 7 (2005) 541–546.
[6] A. Trojánek, J. Langmaier, Z. Samec, Electrochem. Commun. 8 (2006) 475–481.
[7] V.V. Agrawal, N. Varghese, G.U. Kulkarni, C.N.R. Rao, Langmuir 24 (2008) 2494–2500.
[8] K. Yao, W. Lu, X. Li, J. Wang, J. Yuan, Chem. Commun. 49 (2013) 1398–1400.
[9] R.A.W. Dryfe, A. Uehara, S.G. Booth, Chem. Rec. 14 (2014) 1013–1023.
[10] N. Nishi, T. Kakinami, T. Sakka, Chem. Commun. 51 (2015) 13638–13641.
[11] Y. Zhang, N. Nishi, K. Amano, T. Sakka, Electrochim. Acta 282 (2018) 886–891.
[12] M.D. Scanlon, E. Smirnov, T.J. Stockmann, P. Peljo, Chem. Rev. 118 (2018) 3722–3751.
[13] S. Takagi, N. Nishi, T. Sakka, Chem. Lett. 48 (2019) 589–592.
[14] Y. Zhang, N. Nishi, T. Sakka, ACS Appl. Mater. Interfaces 11 (2019) 23731–23740.
[15] Y. Zhang, N. Nishi, T. Sakka, Colloids Surfaces A: Physicochem. Eng. Asp. 597 (2020), 124747.
[16] J. Zhao, C. Jiang, Y. Liu, Aust. J. Chem. 73 (2020) 861–867.
[17] Y. Kuroyama, N. Nishi, T. Sakka, J. Electroanal. Chem. 881 (2021), 114959.
[18] N. Nishi, Y. Kuroyama, N. Yoshida, Y. Yokoyama, T. Sakka, ChemElectroChem 10 (2023) e202201000.
[19] R. Moshrefi, K. Ryan, E.P. Connors, J.C. Walsh, E. Merschrod, G.J. Bodwell, T. J. Stockmann, Nanoscale 15 (2023) 5834–5842.
[20] B.Y. Zheng, Y. Wang, P. Nordlander, N.J. Halas, Adv. Mater. 26 (2014) 6318–6323.
[21] Z.-L. Yang, Q.-H. Li, B. Ren, Z.-Q. Tian, Chem. Commun. 47 (2011) 3909–3911.
[22] J.M. Sanz, D. Ortiz, R. Alcaraz de la Osa, J.M. Saiz, F. González, A.S. Brown, M. Losurdo, H.O. Everitt, F. Moreno, J. Phys. Chem. C 117 (2013) 19606–19615.
[23] B. Cerjan, X. Yang, P. Nordlander, N.J. Halas, ACS Photonics 3 (2016) 354–360.
[24] D.F. Swearer, H. Zhao, L. Zhou, C. Zhang, H. Robatjazi, J.M.P. Martirez, C. M. Krauter, S. Yazdi, M.J. McClain, E. Ringe, E.A. Carter, P. Nordlander, N.J. Halas, Proc. Natl. Acad. Sci. 113 (2016) 8916–8920.
[25] K.J. Smith, Y. Cheng, E.S. Arinze, N.E. Kim, A.E. Bragg, S.M. Thon, ACS Photonics 5 (2018) 805–813.
[26] N. Koura, H. Nagase, A. Sato, S. Kumakura, K. Takeuchi, K. Ui, T. Tsuda, C. K. Loong, J. Electrochem. Soc. 155 (2008) D155–D157.
[27] I. Shitanda, A. Sato, M. Itagaki, K. Watanabe, N. Koura, Electrochim. Acta 54 (2009) 5889–5893.
[28] S. Poges, J. Jin, C. Guild, W.-N. Li, M. Birnkrant, S.L. Suib, Mater. Chem. Phys. 207 (2018) 303–308.
[29] B.D. Clark, C.J. DeSantis, G. Wu, D. Renard, M.J. McClain, L. Bursi, A.-L. Tsai, P. Nordlander, N.J. Halas, J. Am. Chem. Soc. 141 (2019) 1716–1724.
[30] M. Elsharkawi, A.M.K. Esawi, ACS Omega 5 (2020) 5756–5761.
[31] M. Lou, A. Bayles, H.O. Everitt, N.J. Halas, Nano Lett. 22 (2022) 7699–7705.
[32] M. Vraneš, A. Tot, S. Jovanović-Šanta, M. Karaman, S. Dožić, K. Tešanović, V. Kojić, S. Gadžurić, RSC Adv 6 (2016) 96289–96295.
[33] C.J. Dymek, ECS Proc. 1987 (1987) 93–104.
[34] C. Scordilis-Kelley, J. Fuller, R.T. Carlin, J.S. Wilkes, J. Electrochem. Soc. 139 (1992) 694–699.
[35] R. Benn, E. Janssen, H. Lehmkuhl, A. Rufínska, J. Organomet. Chem. 333 (1987) 155–168.
[36] M. Kasuno, Y. Matsuyama, M. Iijima, ChemElectroChem 3 (2016) 694–697.
[37] M. Kasuno, K. Wakabayashi, Y. Matsuyama, R. Yamamura, Electrochim. Acta 343 (2020), 136069.